Multipartite entanglement dynamics in a regular-to-ergodic transition: Quantum Fisher information approach

Karol Gietka,[1] Jan Chwedeńczuk,[1] Tomasz Wasak,[2] and Francesco Piazza[2]
[1]*Faculty of Physics, University of Warsaw, ulica Pasteura 5, 02-093 Warsaw, Poland*
[2]*Max-Planck-Institut für Physik komplexer Systeme, 01187 Dresden, Germany*

(Received 10 December 2018; published 21 February 2019)

The characterization of entanglement is a central problem for the study of quantum many-body dynamics. Here, we propose the quantum Fisher information (QFI) as a useful tool for the study of multipartite-entanglement dynamics in many-body systems. We illustrate this by considering the regular-to-ergodic transition in the Dicke model—a fully connected spin model showing quantum thermalization above a critical interaction strength. We show that the QFI has a rich dynamical behavior which drastically changes across the transition. In particular, the asymptotic value of the QFI as well as its characteristic timescales witness the transition both through their dependence on the interaction strength and through the scaling with the system size. Since the QFI also sets the ultimate bound for the precision of parameter estimation, it provides a metrological perspective on the characterization of entanglement dynamics in many-body systems. Here, we show that quantum ergodic dynamics allows for a much faster production of metrologically useful states.

DOI: 10.1103/PhysRevB.99.064303

I. INTRODUCTION

A thorough understanding of quantum many-body dynamics necessarily requires the study of the time evolution of the entanglement between the particles. In recent years, several studies have been performed especially in the context of thermalization in closed quantum many-body systems [1–6]. The computation of entanglement in strongly correlated systems is a challenging task, and a few general results are available for given system subclasses, such as for the time evolution of entanglement entropy in one-dimensional systems [7] and ergodic systems [8,9], or the boundary laws for asymptotic states of local Hamiltonians [10]. The logarithmic growth in the time of entanglement entropy has provided a clear distinction between Anderson and many-body localization [11–15]. Whereas throughout these studies the entanglement is mostly characterized using bipartite entanglement entropies (which can be applied only to closed systems in pure quantum states), the interest in alternative measures has recently emerged [16–19].

In this paper, we propose the quantum Fisher information (QFI) [20,21] as a useful quantity for the study of the time evolution of entanglement in many-body systems. The QFI is a measure of genuine multipartite entanglement [22–26]. With respect to entanglement entropies, it has the important advantage of being directly applicable to mixed states and, thus, to open-system dynamics. It is widely studied in the context of quantum metrology—as it sets a lower bound for the uncertainty in parameter estimation—but much less for the characterization of the dynamics of quantum many-body systems. So far, the QFI has been used to detect phase transitions in ground or thermal states [27–29], whereas its dynamical behavior across phase transitions remains largely unexplored, in particular, in ergodic systems.

Here, we show that the QFI provides a very rich characterization of quantum many-body dynamics across a regular to ergodic transition. We consider the Dicke model (DM) where interactions between N spin-$(1/2)$ particles are mediated by a bosonic mode coupled at a rate g [30,31] (see also Fig. 1). As shown by Altland and Haake [32,33], the Dicke model offers a paradigm for quantum thermalization dynamics with underlying classical chaos in a fully connected system. In particular, the semiclassical dynamics in phase space shows a transition between regular and ergodic at a critical coupling strength g_c, consistent with the behavior of the Hamiltonian spectrum turning from Poissonian to Wigner-Dyson level statistics [34].

We find that the QFI in the DM has a dynamical behavior which drastically changes across the transition between the regular and the ergodic phases. Its asymptotic value as well as the characteristic timescales witness the transition both through their dependence on the control parameter g and through their scaling with system's size N.

II. SUMMARY OF THE MAIN RESULTS

Starting from a state which is not an eigenstate of the DM Hamiltonian [see Eq. (13)] and fixing the initial energy with respect to the ground state (see Fig. 2), we compute the time evolution of the QFI optimized over all possible atomic single-particle operations. In the regular phase $g < g_c$ (see Fig. 3 bottom row), the QFI shows oscillations around an envelope which grows continuously in time as $\mathrm{erf}(t^2/t_{\mathrm{asy}}^2)$ and asymptotically at $t \simeq t_{\mathrm{asy}}$ saturates to a value scaling at the Heisenberg limit (HL) $\propto N^2$. The latter is the strongest possible scaling for a system of N qubits. On the other hand, in the ergodic phase $g > g_c$ (see Fig. 3, upper row), the QFI envelope first reaches an intermediate plateau with shot-noise

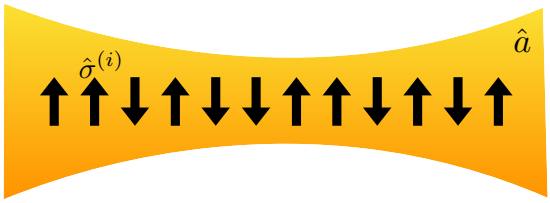

FIG. 1. Graphical illustration of the Dicke model [see Eq. (13)] studied in this paper. N spins of length $1/2$ are all coupled to a single bosonic mode.

(SN) scaling $\propto N$ within a time $t_{\rm pla} < t_{\rm asy}$, and only after $t_{\rm asy}$ reaches its final asymptotic value, the latter again showing Heisenberg scaling. This double-step growth in the ergodic phase disappears at high enough initial energies (see Fig. 4) where the QFI envelope grows like $\mathrm{erf}(t^2/t_{\rm asy}^2)$ for all values of g.

Although the asymptotic value of the QFI scales at the HL both in the ergodic and in the regular phase (see Fig. 5), its actual value shows a sharp behavior at the critical coupling strength g_c after which it rapidly grows (see the blue points in Fig. 6). Its behavior for $g = g_c$, however, becomes less sharp as energy is increased (see the red triangles in Fig. 6).

Also, the timescale $t_{\rm asy}$ witnesses the transition as it abruptly drops by increasing g down until g_c after which it saturates to a constant value (see Fig. 7). Remarkably, the behavior of $t_{\rm asy}$ as a function of g is almost independent of the initial energy (compare the red triangles and blue points in Fig. 7). Therefore, different from the asymptotic value, the saturation time $t_{\rm asy}$ remains a good witness of the regular-to-ergodic transition at all energies.

The system-size dependence of the timescales is also clearly distinct in the two phases: in the regular phase $t_{\rm asy} \propto \sqrt{N}$, whereas in the ergodic phase the scaling of $t_{\rm asy}$ is

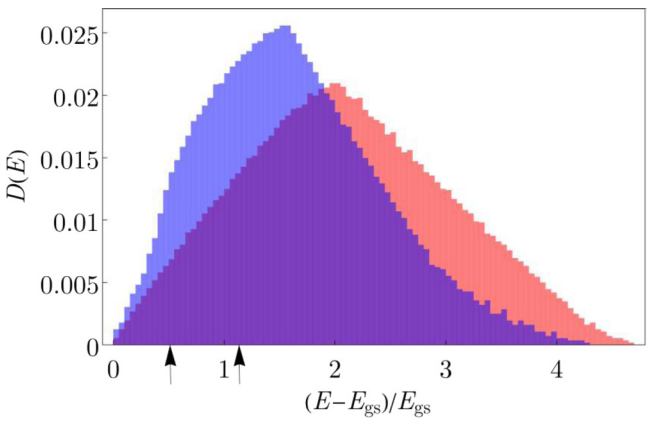

FIG. 2. Density of states as a function of $(E - E_{\rm gs})/E_{\rm gs}$ for the Hamiltonian (13) for $N = 100$ and $g = 0.3$ (red, right peak) or $g = 0.9$ (blue, left peak). Arrows indicate the two different initial energies which are compared throughout the following analysis. The density of states on the right of the peak converges slowly with the cutoff in the bosonic Fock space. In our case, we choose it such that the density of states converged in the whole region on the left of the peak. This guarantees that our numerical results are independent of the cutoff.

consistent with $\ln(N)$, at least, at high-enough initial energies (see Fig. 8). The fact that $t_{\rm asy} \propto \ln(N)$ suggest its interpretation as the Ehrenfest time, which is proportional to the volume of the accessible phase space, the latter being proportional to N in the DM [33].

This interpretation is confirmed by an analysis of the Wigner distribution function, according to which $t_{\rm pla}$ is connected to the formation of weakly squeezed nonclassical states whereas $t_{\rm asy}$ corresponds to the distribution fully covering the available region of phase space and forming small-scale structures of angular size $1/N$. The size of the region covered by the Wigner distribution quickly grows by increasing the initial energy until the whole phase space is taken, consistent with the prediction of Altland and Haake for the Husimi function [32] and the underlying classical chaos (see Fig. 9 and 10). As discussed above, at such initial energies, the double-step growth of the QFI is absent. Such a double-plateau formation can thus be related to the mixed character of the underlying classical phase space.

Upon a QFI-based characterization of many-body dynamics, one obtains a quantification of the usefulness of the given many-body state for quantum metrology since the lower bound to the uncertainty of parameter estimation is set by the inverse square root of the QFI [35]. For instance, recent studies have demonstrated the metrological usefulness of quantum states generated during chaotic dynamics in the kicked top [36]. Our results here show that, compared to regular dynamics, quantum ergodic dynamics allows for a much faster production of entangled many-body states providing Heisenberg scaling of the metrological precision.

III. QUANTUM FISHER INFORMATION AND MULTIPARTITE ENTANGLEMENT

In this section, we will summarize the properties of the QFI which are relevant for the following analysis and discussion.

For a quantum state given by a density-matrix $\hat{\varrho}$, the QFI is defined in relation to a chosen Hermitian operator $\hat{O}$, called the generator of the transformation as

$$I^{Q}[\hat{\varrho};\hat{O}] = 2\sum_{l,l'}\frac{(\lambda_l-\lambda_{l'})^2}{\lambda_l+\lambda_{l'}}|\langle l|\hat{O}|l'\rangle|^2\,, \tag{1}$$

with the spectral decomposition of the density matrix given by $\hat{\varrho} = \sum_l \lambda_l |l\rangle\langle l|$, where $\lambda_l > 0$ and $\sum_l \lambda_l = 1$. For pure states, the QFI reduces to $I^{Q} = 4(\Delta\hat{O})^2 = 4(\mathrm{Tr}[\hat{\varrho}\hat{O}^2] - \mathrm{Tr}[\hat{\varrho}\hat{O}]^2)$, i.e., four times the variance of the operator. The QFI can be interpreted as a square of a "statistical speed" [20,21], defined as the rate of change in the absolute statistical distance between two quantum states along a single-parameter path generated by the operator $\hat{O}$ through

$$\hat{\varrho}(\theta) = e^{-i\theta\hat{O}}\hat{\varrho}e^{i\theta\hat{O}}. \tag{2}$$

For thermal states, the QFI coincides with the dynamic susceptibility related to the operator $\hat{O}$ [27].

In our paper, the QFI is used as a mean to characterize multipartite entanglement. In the particular case of the DM considered here [see Eq. (13)], we have a composite Hilbert space made of a bosonic degree of freedom (L) and a spin subsystem (S) made of N spins of length $1/2$. The total Hilbert

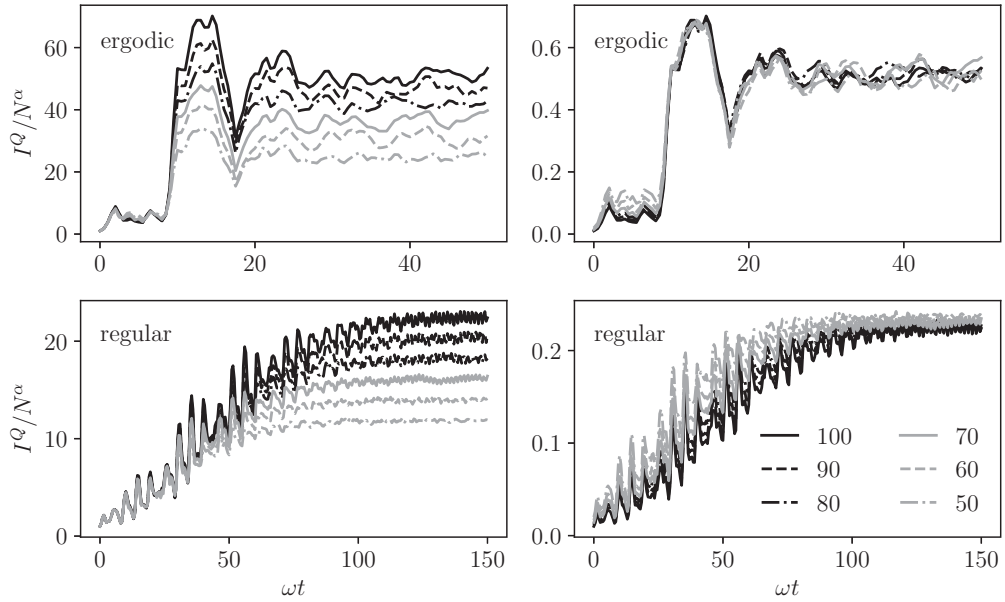

FIG. 3. Dynamics of the QFI in the ergodic (top row) vs regular phase (bottom row). To render the different scaling regimes apparent, the QFI I^Q/N^α is shown for different system sizes N (ranging from 50 to 100 with $\Delta N = 10$) for $\alpha = 1$ (left column) and $\alpha = 2$ (right column). Hereinafter, the parameters are expressed in units of ω, and the energy of the initial state is fixed with respect to the ground state, i.e., $(E - E_{\rm gs})/E_{\rm gs} = 0.53$ (see also Fig. 2). Here, $\omega_0 = 1$, $g = 0.9$ (top row), and $g = 0.4$ (bottom row).

space is a tensor product of the two subspaces,

$$\mathcal{H} = \mathcal{H}_{\rm L} \otimes \mathcal{H}_{\rm S}. \tag{3}$$

We focus on pure states of the composite system, i.e., $|\Psi\rangle \in \mathcal{H}$ and concentrate on the multipartite entanglement in the spin subspace. We consider the following *linear* (in a sense that no products of $\hat{\vec{\sigma}}^{(l)}$ and $\hat{\vec{\sigma}}^{(l')}$ appear) operators,

$$\hat{O}_{\rm lin} = \hat{\mathbb{I}}_{\rm L} \otimes \frac{1}{2} \sum_{l=1}^{N} \vec{n}^{(l)} \cdot \hat{\vec{\sigma}}^{(l)}, \tag{4}$$

with the Pauli operators $\hat{\vec{\sigma}}^{(l)} = (\hat{\sigma}_x^{(l)}, \hat{\sigma}_y^{(l)}, \hat{\sigma}_z^{(l)})$ and the vectors $\vec{n}^{(l)} = (n_x^{(l)}, n_y^{(l)}, n_z^{(l)})$ that define the rotation of the Bloch sphere such that $(n_x^{(l)})^2 + (n_y^{(l)})^2 + (n_z^{(l)})^2 = 1$. The only possible pure state $|\Psi\rangle$ in which the spins and bosons are nonentangled is of the form

$$|\Psi\rangle = |\psi\rangle_{\rm L} \otimes |\phi_1\rangle \otimes |\phi_2\rangle \cdots \otimes |\phi_N\rangle, \tag{5}$$

where $|\psi\rangle_{\rm L}$ is a state of the bosonic subsystem and $|\phi_i\rangle$ is a state of the ith single spin. If all the spins are in the same state,

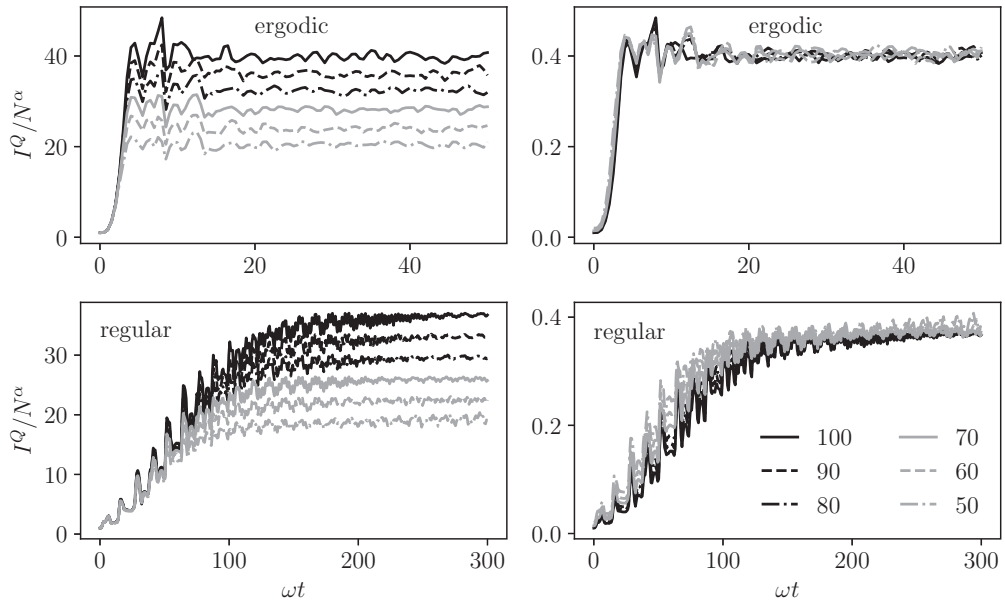

FIG. 4. The same as in Fig. 3, this time for a higher initial energy $(E - E_{\rm gs})/E_{\rm gs} = 1.11$ (see also Fig. 2).

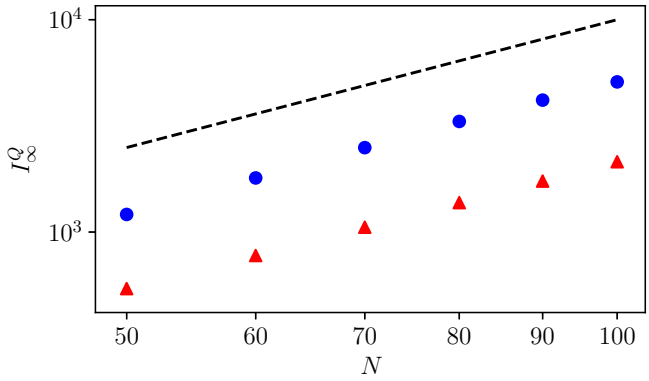

FIG. 5. Asymptotic value I^Q_∞ of the QFI as a function of N in double-logarithmic scale for $g = 0.9$ (blue curve) and $g = 0.4$ (red curve). The black dashed curve is the HL, i.e., $I^Q_\infty = N^2$. Here, the initial energy is $(E - E_{\rm gs})/E_{\rm gs} = 0.53$.

the N-body state $|\phi\rangle^{\otimes N}$ is called the coherent spin state (CSS). For nonentangled states and the transformation (4), the QFI is bounded by

$$I^Q[|\Psi\rangle; \hat{O}_{\rm lin}] = 4(\Delta \hat{O}_{\rm lin})^2 \leqslant N, \tag{6}$$

i.e., the shot-noise limit (SNL) [22]. This bound can be overcome when the spins are entangled. To see this, consider an exemplary state,

$$|\Psi\rangle = \frac{1}{\sqrt{2}}(|0\rangle \otimes |\uparrow\rangle^{\otimes N} + |1\rangle \otimes |\downarrow\rangle^{\otimes N}), \tag{7}$$

where $|0\rangle$ and $|1\rangle$ are a bosonic vacuum and a one-particle state, respectively, and $|\uparrow\rangle/|\downarrow\rangle$ are the eigenstates of $\hat{\sigma}_z$ with eigenvalues ± 1. Taking now

$$\hat{O}_{\rm lin} = \hat{\mathbb{I}}_{\rm L} \otimes \hat{J}_z, \tag{8}$$

with the collective angular momentum operators of N spins defined as

$$\hat{J}_{\vec{n}} = \frac{1}{2}\vec{n} \cdot \left(\sum_{l=1}^{N} \hat{\vec{\sigma}}^{(l)}\right) \tag{9}$$

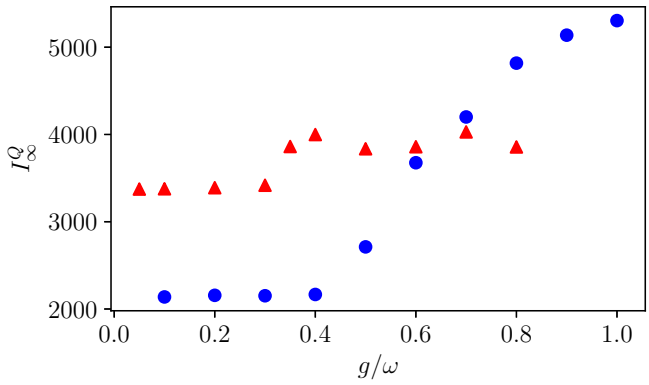

FIG. 6. Asymptotic value I^Q_∞ of the QFI across the regular-to-ergodic transition. Here, $N = 100$, and the initial energy $(E - E_{\rm gs})/E_{\rm gs} = 0.53$ (blue dots) or $(E - E_{\rm gs})/E_{\rm gs} = 1.11$ (red triangles).

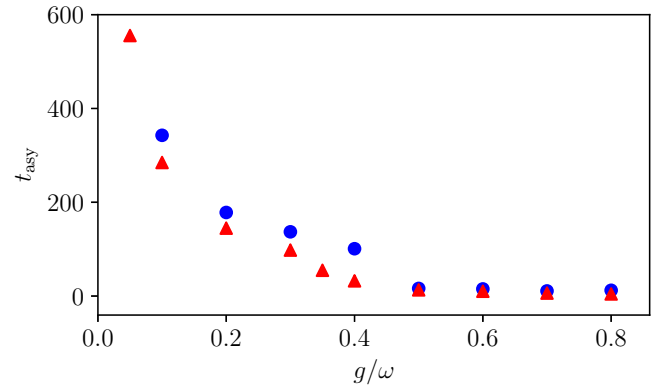

FIG. 7. Behavior of the saturation time $t_{\rm asy}$ across the regular-to-ergodic transition. Here, $N = 100$, and the initial energy $(E - E_{\rm gs})/E_{\rm gs} = 0.53$ (blue dots) or $(E - E_{\rm gs})/E_{\rm gs} = 1.11$ (red triangles).

we obtain

$$I^Q[|\Psi\rangle; \hat{O}_{\rm lin}] = N^2, \tag{10}$$

which is the HL and is the maximal value of the QFI for the family of linear transformations (4). The example (7) can also be used to illustrate one additional property of the QFI for transformations (4). Taking the reduced density matrix of spins, obtained after tracing out the bosonic degree of freedom from the state (7), we obtain

$$\hat{\varrho}_{\rm S} = {\rm Tr}[|\Psi\rangle\langle\Psi|]_{\rm L} = \tfrac{1}{2}[(|\uparrow\rangle\langle\uparrow|)^{\otimes N} + (|\downarrow\rangle\langle\downarrow|)^{\otimes N}]. \tag{11}$$

This is a separable (nonentangled) state for which the QFI calculated from Eq. (1) gives $I^Q \leqslant N$ for any $\hat{J}_{\vec{n}}$, thus, the SNL [22].

To summarize, the QFI calculated with the operators (4) is more than just a criterion for the entanglement between

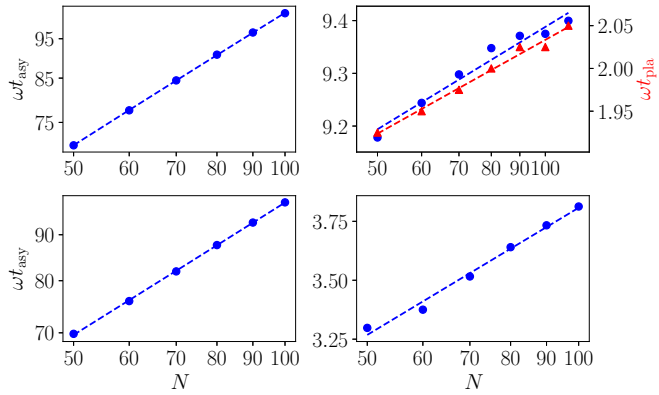

FIG. 8. Behavior of the timescales as a function of system size in the regular ($g = 0.3$, left column, double-logarithmic scale) vs ergodic phase (here $g = 0.9$, right column, semilogarithmic scale) for initial energies $(E - E_{\rm gs})/E_{\rm gs} = 0.53$ (upper row) and $(E - E_{\rm gs})/E_{\rm gs} = 1.11$ (bottom row). Dashed lines are guides to the eye. In the regular phase the asymptotic time $t_{\rm asy}$ is well fitted by $\sqrt{N}$. In the the ergodic phase the scaling is consistent with $\ln(N)$ for $(E - E_{\rm gs})/E_{\rm gs} = 1.11$. This is less clear at $(E - E_{\rm gs})/E_{\rm gs} = 0.53$, where we also show the scaling of the intermediate-plateau time $t_{\rm pla}$.

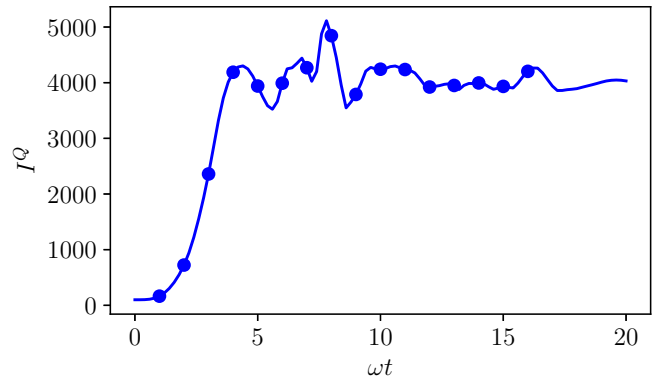

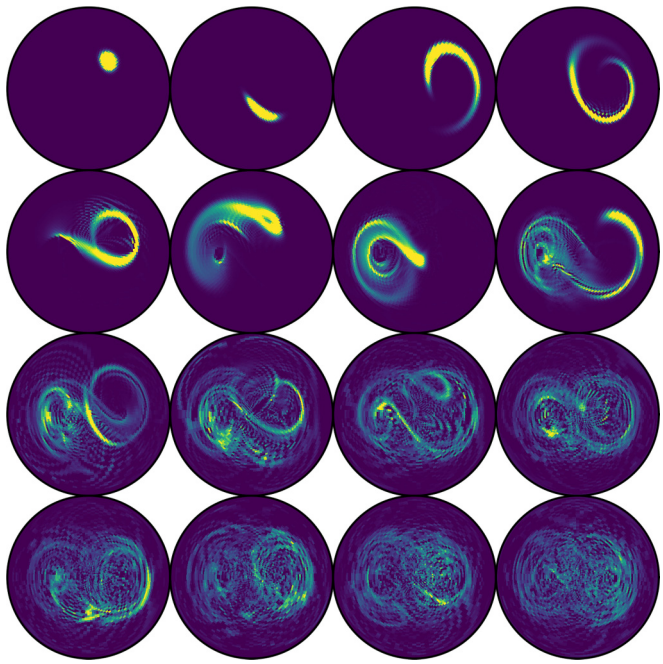

FIG. 9. Time evolution of the Wigner phase-space distribution in the ergodic phase at large energies. Points on the I^Q curve are the points at which we calculate the Wigner function of the state. Here, $N = 100$ and the remaining parameters are the same as in Fig. 5, i.e., $(E - E_{gs})/E_{gs} = 1.11,\ g = 0.9$.

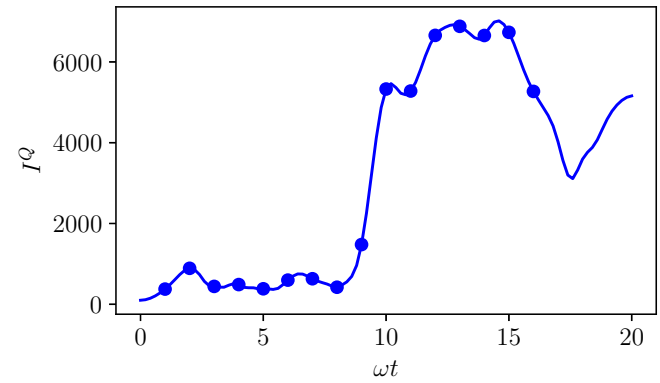

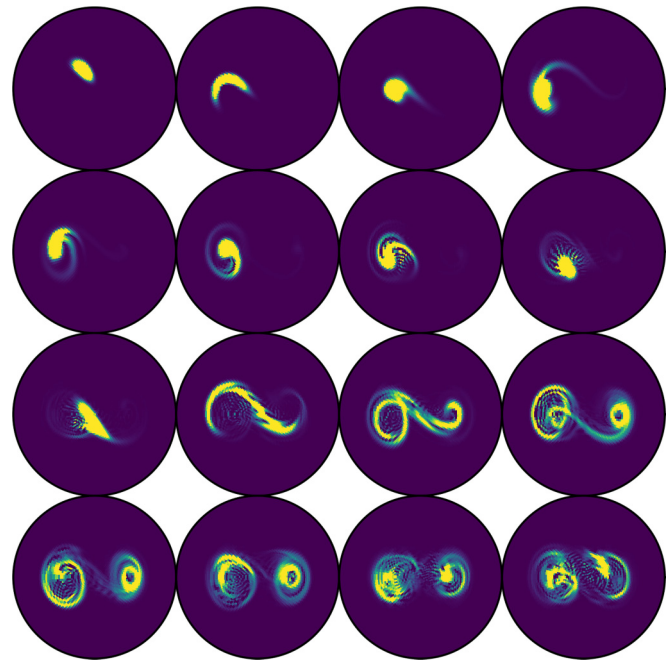

FIG. 10. The same as in Fig. 9, except that now there parameters are as follows: $(E - E_{gs})/E_{gs} = 0.53$ and $g = 0.9$ (cf. Fig. 3).

spins. It rather detects the entanglement within the spin subspace of the full many-body state $|\Psi\rangle \in \mathcal{H}$, that is, either we have entangled spins classically correlated with the bosons or nonentangled spins non-classically correlated with bosons.

We stress that the QFI is an experimentally accessible quantity even in systems of many qubits as recently demonstrated with ultracold atoms [37,38]. Also, in view of the recent proposals for an efficient QFI witnessing [39–41], the extensions to more complex and larger systems seems a concrete possibility in the near future.

For the following analysis of multipartite-entanglement dynamics, we will compute the QFI for the momentary quantum state and maximize it at every instant in time with respect to all possible operators of the class (4).

As the DM Hamiltonian (13) is fully connected and, thus, contains only collective angular momentum operators of the type (9), it is sufficient to consider the following optimized QFI:

$$I^Q(t) = \max_{\vec{n}} I^Q[\hat{\varrho}(t); \hat{\mathbb{I}}_L \otimes J_{\vec{n}}], \tag{12}$$

which reduces the maximization problem to finding the optimal vector $\vec{n}$ defining the rotation axis. Here, $\hat{\varrho}(t) = \hat{U}(t)\hat{\varrho}_0\hat{U}^\dagger(t)$, $\hat{\varrho}_0$ being the initial state and $\hat{U}(t)$ the unitary evolution operator generated by the Hamiltonian.

We note that $I^Q(t)$ is *not* related to an echo fidelity [42]—an important quantity in the context of thermalization and irreversibility which has been studied also for the Dicke model [43]—since in our case the path in density-matrix space is not generated by the time-evolution operator $\hat{U}(t)$ but rather by $\hat{O}_{lin}$ at every instant in time.

Finally, we point out that the QFI also provides ultimate bounds for the precision of estimation of a metrological parameter θ under the transformation (2). Accordingly, the bound for the uncertainty of the parameter estimation is $\Delta\theta \geqslant I^Q[\hat{\varrho}; \hat{O}_{lin}]^{-1/2}$. Separable states at most achieve the SNL sensitivity whereas maximally entangled states can, in principle, yield the HL precision [20,22,35].

IV. MODEL AND APPROACH

A paradigmatic feature of generic many-body systems is ergodicity, that is, the ability to relax to an asymptotic state which can be effectively described by thermal equilibrium. For closed quantum systems, the issue of thermalization—and its absence, for instance, due to integrability or disorder—is still an object of intensive study [1–6]. With the aim of putting forward the QFI for the characterization of many-body dynamics, we consider here the Dicke model [30,31], which is one of the simplest instances of a quantum many-body system showing thermalization. Its Hamiltonian is given by (setting $\hbar = 1$),

$$\hat{H} = \omega_0 \hat{J}_z + \omega \hat{a}^\dagger \hat{a} + \frac{2g}{\sqrt{N}}(\hat{a} + \hat{a}^\dagger)\hat{J}_x. \tag{13}$$

The simplicity of the DM resides in it being a fully connected model—only the collective spin operators $\hat{J}_{\vec{n}}$ appear in Eq. (13)—with interactions between the N spin-(1/2) particles mediated by a single bosonic degree of freedom $\hat{a}$ satisfying $[\hat{a}, \hat{a}^\dagger] = 1$.

The DM features a second-order phase transition in the ground state at the critical coupling $g_c = 0.5$, above which the average value of the total magnetization $\langle \hat{J}_x \rangle$ as well as the coherent contribution to the bosonic field $\langle \hat{a} \rangle$ become finite thereby spontaneously breaking the Z_2 symmetry of the Hamiltonian (13): $\hat{a} \to -\hat{a}$, $\hat{J}_x \to -\hat{J}_x$. What is more relevant for the present paper is that at $g = g_c$ also the whole spectrum of eigenstates changes: The level statistics, namely, shows a transition from Poissonian below g_c to Wigner-Dyson above [34]. This indicates that the DM should behave ergodically above g_c. Indeed, this is confirmed by the semiclassical analysis of [32,33], showing that in this case a state initially localized in phase space eventually covers homogeneously the whole phase space available at the initially fixed energy, that is, the system relaxes to a microcanonical distribution. A semiclassical study of the DM is justified as a perturbative expansion in $1/N$ since the fully connected nature makes it such that the DM possesses a classical limit for $N \to \infty$. The classical dynamics shows a crossover from regular to chaotic which can be connected to the thermalizing behavior of the full quantum model.

Our aim is to study the entanglement dynamics in the DM at finite N using the QFI, with particular attention to the characterization of the transition from regular to ergodic behavior as a function of g.

V. RESULTS

We compute the time evolution of the optimized QFI $I^Q(t)$ defined in Eq. (12) by starting from an initial pure state $|\Psi_0\rangle$ with an initial energy $E = \langle \Psi_0 | \hat{H} | \Psi_0 \rangle$. While changing the coupling strength g and the number of spins N, we keep the ratio of the initial energy to the ground-state energy $E_{\rm gs}$ fixed. In the following, we present results for two different energy ratios corresponding to the arrows shown in Fig. 2. We pick the initial state to be $|\Psi_0\rangle = |\alpha\rangle \otimes |\phi\rangle^{\otimes N}$, i.e., the product of a coherent state of the bosons $\hat{a}|\alpha\rangle = \alpha|\alpha\rangle$ and a CSS for the spins (in the Appendix, we also present results for a weakly correlated spin-squeezed state). This is not an eigenstate of the DM-Hamiltonian (13), and we fix its average energy by choosing the CSS of spins and adjusting the value of α.

A. QFI dynamics

The time evolution of the optimized QFI is shown in Figs. 3 and 4 for the two different initial energies. In each figure, we compare the typical dynamics below and above g_c. Based on the behavior of the level statistics [34] discussed in Sec. IV, we will refer to the parameter region $g < g_c$ as the regular phase and to the region $g > g_c$ as the ergodic phase. In all cases, the QFI shows oscillations around an envelope, the latter growing in time until it reaches a stationary asymptotic value I^Q_∞ within a timescale $t_{\rm asy}$. In the regular phase (bottom row of Figs. 3 and 4), the QFI envelope grows steadily and is well fitted by

$$I^Q_{\rm env}(t) = I^Q_0 + \left(I^Q_\infty - I^Q_0\right) \mathrm{erf}\left(\frac{t^2}{t^2_{\rm asy}}\right), \tag{14}$$

where erf is the error function. On the other hand, in the ergodic phase the QFI shows a two-step growth, first reaching an intermediate plateau within a time $t_{\rm pla}$ and then suddenly abandoning it to reach its asymptotic value for $t > t_{\rm asy}$. This two-step growth, however, disappears at high enough energies as shown in Fig. 4 where the intermediate plateau is absent, and the QFI envelope is always well fitted by the functional form (14).

B. Asymptotic value

In Figs. 3 and 4, we present two different rescalings of the QFI: The left panels show I^Q/N whereas the right panels show I^Q/N^2. First, we observe that the asymptotic value I^Q_∞ always scales, such as N^2 as indicated by the overlapping curves for $t > t_{\rm asy}$ in all the right panels, independent of the coupling strength and the initial energy. This is shown more directly in Fig. 5, where I^Q_∞ is plotted as a function of N both in the regular and in the ergodic phase. We note that I^Q_∞ scales with N, such as the HL but lies below the ultimate bound by a numerical prefactor $\sim 1/2$. On the other hand, the upper-left panel of Fig. 3 shows that the QFI in the intermediate plateau appearing for $t_{\rm pla} < t < t_{\rm asy}$ scales, such as N, i.e., such as the SNL.

The scaling of the asymptotic value I^Q_∞ with the system's size N does not allow to distinguish the regular from the ergodic phase. However, the behavior of I^Q_∞ as a function of the coupling strength g can much better distinguish the two phases. As shown in Fig. 6, for $(E - E_{\rm gs})/E_{\rm gs} = 0.53$ the asymptotic value shows a sharp transition at $g = g_c = 0.5\omega$. I^Q_∞ is, namely, almost constant below g_c and suddenly grows above. This behavior however becomes less and less sharp as the initial energy grows as testified by the red triangles in Fig. 6 at $(E - E_{\rm gs})/E_{\rm gs} = 1.11$. By increasing the initial energy, not only the value of I^Q_∞ increases in the regular phase, but it also decreases in the ergodic phase. Moreover, the value of g at which I^Q_∞ starts appreciably growing is slightly moved to lower g [44].

C. Characteristic timescales

The timescales characterizing the dynamics of the QFI constitute an even better witness of the regular-to-ergodic transition. As shown in Fig. 7, the time $t_{\rm asy}$ required for the QFI to reach its asymptotic value quickly decreases by increasing the coupling strength g until the latter reaches g_c [45]. Upon entering the ergodic phase for $g > g_c$, $t_{\rm asy}$ settles to an essentially constant value. Remarkably, this sharp behavior across g_c is present independent of the initial energy, as apparent from comparing the red triangles and the blue circles in Fig. 7. In particular, the fact that the time required for the multipartite entanglement measured by the QFI to saturate does not depend on the interaction strength seems a good indicator for the ergodic character of the system.

The regular and the ergodic phase can also be distinguished by the scaling of the saturation time $t_{\rm asy}$ with the system's size N as shown in Fig. 8. In the regular phase, the dependence of $t_{\rm asy}$ on N is very well fitted by $\sqrt{N}$. This holds independently of the initial energy as one can see in the left panels of Fig. 8. In the ergodic phase instead the scaling of $t_{\rm asy}$ is consistent with $\ln(N)$ (see lower right panel of Fig. 8). On a qualitative level, this implies that in approaching the thermodynamic limit with our fully connected model, the time required to reach the asymptotic, HL-scaling value of the entanglement diverges much slower with system size in the ergodic phase.

On the other hand, in the ergodic phase but at low enough energies we have seen that an intermediate plateau appears between $t_{\rm pla}$ and $t_{\rm asy}$. In the upper right panel of Fig. 8 we see that in this case the scaling of $t_{\rm asy}$ and $t_{\rm pla}$ with the system's size is not as well fitted by $\ln(N)$, at least, for the sizes we explore here. This might be due to the mixed nature of the underlying classical phase space as we discuss in the next section.

D. Wigner distribution

The logarithmic-scaling with the system size of the saturation time $t_{\rm asy}$ in the ergodic phase suggests an interpretation as an Ehrenfest time. The latter is related to the breakdown of the semiclassical description of the dynamics, and the time at which this happens is known to scale as the logarithm of the volume of the available phase space. This, in turn, for the DM depends linearly on N, and so the Ehrenfest timescales as $\ln N$ [33].

We validate this hypothesis by analyzing the dynamics of the $SU(2)$ Wigner distribution, defined by [46]

$$W(\theta,\phi) = \sum_{k=0}^{2j} \sum_{q=-k}^{k} Y_{kq}(\theta,\phi) G_{kq}, \tag{15}$$

where Y_{kq} are the spherical harmonics and G_{kq} are expansion coefficients in the basis of multipole operators $\hat{T}_{kq}$ [47] of the reduced density matrix for the spin subsystem $\hat{\varrho}_{\rm S}(t) \equiv {\rm Tr}_{\rm L}[|\Psi\rangle\langle\Psi|]$:

$$\hat{\varrho}_{\rm S} = \sum_{k=0}^{2j} \sum_{q=-k}^{k} G_{kq} \hat{T}_{kq}. \tag{16}$$

The above Wigner function is defined on the phase space of the spin degrees of freedom spanned by two angles θ, ϕ.

The asymptotic plateau reached after $t_{\rm asy}$ is characterized by the QFI scaling, such as the HL $\propto N^2$, i.e., maximal entanglement (reduced by a prefactor $\sim 1/2$, see Fig. 4). Correspondingly, the Wigner function shown in Fig. 10 (in azimuthal equidistant projection) quickly spreads over a larger portion of the phase space, ultimately covering it fully for high-enough initial energy. While spreading over phase space, the Wigner function forms small-scale structures of characteristic size $1/N$ as expected from ergodic quantum systems [48]. This small-scale structures in phase space are responsible for the scaling with N^2 of the QFI [22].

On the other hand, we have seen that at lower initial energies that the QFI reaches first an intermediate plateau within the time $t_{\rm pla}$. Here, the value of $I^Q(t)$ is larger than the SNL but still scales, such as N (see upper row of Fig. 3 and recall that the initial state is not entangled). As the Wigner function in Fig. 9 shows, the intermediate plateau corresponds indeed to the creation of a slightly squeezed state which rotates without spreading until the time $t_{\rm asy}$ is reached. Around $t = t_{\rm asy}$, the Wigner function suddenly spreads into a bimodal distribution. The latter does not isotropically cover the available region of phase space, which can be related to the mixed character of the underlying classical dynamics [33]. One might suppose that this is also the reason why the characteristic timescales here do not seem to be scaling as the logarithm of the system size, see upper right panel of Fig. 8.

VI. CONCLUSIONS

Using the QFI, we studied the dynamics of multipartite entanglement in a fully connected quantum many-body system across a regular-to-ergodic transition. The QFI allows to sharply distinguish the ergodic from the regular phase, as its asymptotic value, as well as the characteristic timescales, witness the transition both through their dependence on the control parameter g and through their scaling with system's size N.

The next set of investigations should involve the extension of the present analysis to many-body systems with finite-range interactions and in the presence of disorder (where some results for QFI dynamics in such systems have recently been discussed in the context of disordered ion chains [49]) and in contact with external baths.

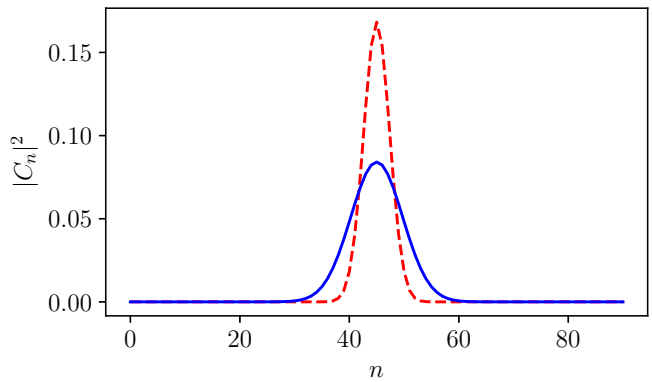

FIG. 11. The comparison between a coherent spin state (solid blue line) and a weakly correlated spin-squeezed state (dashed red line). Here, $N = 90$ and $\sigma^2 = 0.25$.

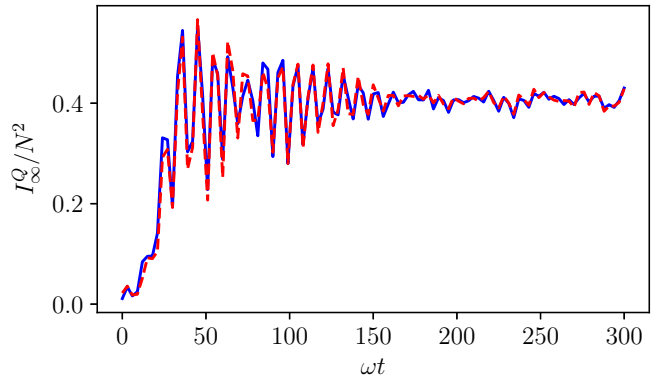

FIG. 12. Regular QFI dynamics normalized to N^2 for the initially classical state (solid blue curve) and the initially weakly spin-squeezed state (dashed red curve). Here, $N = 90$, $(E - E_{\rm gs})/E_{\rm gs} = 1.11$, and $g = 0.4$.

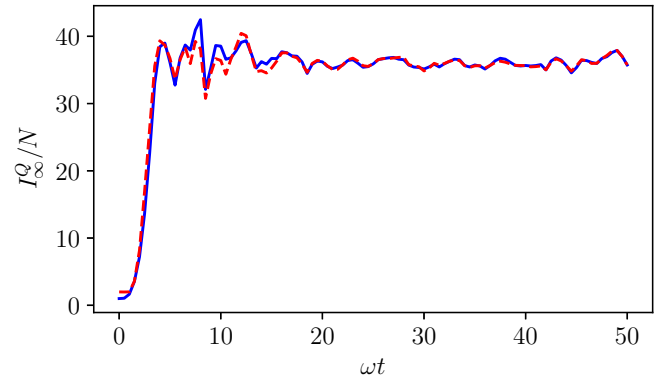

FIG. 13. Ergodic QFI dynamics normalized to N for the initially classical state $\sigma^2 = 1$ (solid blue curve) and the initially weakly spin-squeezed state $\sigma^2 = 0.25$ (dashed red curve). Here, $N = 90$, $(E - E_{\rm gs})/E_{\rm gs} = 1.11$, and $g = 0.9$.

ACKNOWLEDGMENTS

We are grateful to D. Luitz for useful discussions and comments. Simulations were performed using the open-source framework in JULIA [50] (see Ref. [51]); K.G. is grateful to D. Plankensteiner for related discussions. K.G. acknowledges financial support from the National Science Centre Poland (NCN) under the ETIUDA scholarship (Grant No. 2017/24/T/ST2/00161).

APPENDIX: INITIALLY CORRELATED SPINS

To check the how initial correlations between the spins change the behavior of the entanglement dynamics, we use the initial state in the form

$$|\psi(\sigma)\rangle = \mathcal{N}\sum_{n=0}^{N} e^{-(n-N/2)^2/(N\sigma^2)}|n - N/2\rangle. \tag{A1}$$

Here, $\mathcal{N}$ is the normalization constant, and $|n - N/2\rangle$ is the Dicke state. The width σ controls the population imbalance fluctuations according to $\sigma^2 \simeq 4(\Delta\hat{J}_z^2)^2/N$. When these fluctuations drop below the shot-noise level, i.e., $\sigma^2 < 1$, the parameter $\xi^2 = N(\Delta\hat{J}_z)^2/\langle\hat{J}_x\rangle^2$ drops below unity, and the spins are spin squeezed [25,52]. In turn, $\xi^2 < 1$ implies that the spins are entangled [53].

To picture the impact of the initial entanglement between the spins, we run a simulation for a state with $\sigma^2 = 1$ (nonentangled) and $\sigma^2 = 0.25$ (spin squeezed and entangled) for the regular and the ergodic dynamics. Figure 11 shows the probabilities $|C_n|^2$ for finding the spins in a given Dicke state $|n - N/2\rangle$ for these two cases. The dynamics of the QFI for $\sigma^2 = 1$ and $\sigma^2 = 0.25$ is compared in Figs. 12 and 13.

From the presented figures, we observe that initiating the simulation with a weakly correlated state gives rise only to small quantitative changes at short-time scales. We expect that a highly correlated initial state, for example, the optimally spin-squeezed state should reduce the characteristic timescales. However, taking into account the types of possible correlations—classical, quantum, or both—and the carrier of correlations–spins, field, or both—we cannot simply infer on any further quantitative or qualitative changes in the dynamics. We defer this issue to future work.

[1] J. M. Deutsch, Quantum statistical mechanics in a closed system, Phys. Rev. A **43**, 2046 (1991).

[2] M. Srednicki, Chaos and quantum thermalization, Phys. Rev. E **50**, 888 (1994).

[3] M. Rigol, V. Dunjko, and M. Olshanii, Thermalization and its mechanism for generic isolated quantum systems, Nature (London) **452**, 854 (2008).

[4] J. Eisert, M. Friesdorf, and C. Gogolin, Quantum many-body systems out of equilibrium, Nat. Phys. **11**, 124 (2015).

[5] F. Borgonovi, F. M. Izrailev, L. F. Santos, and V. G. Zelevinsky, Quantum chaos and thermalization in isolated systems of interacting particles, Phys. Rep. **626**, 1 (2016).

[6] D. J. Luitz and Y. Bar Lev, Anomalous Thermalization in Ergodic Systems, Phys. Rev. Lett. **117**, 170404 (2016).

[7] P. Calabrese and J. Cardy, Evolution of entanglement entropy in one-dimensional systems, J. Stat. Mech.: Theor. Exp. (2005) P04010.

[8] H. Kim and D. A. Huse, Ballistic Spreading of Entanglement in a Diffusive Nonintegrable System, Phys. Rev. Lett. **111**, 127205 (2013).

[9] D. J. Luitz, N. Laflorencie, and F. Alet, Extended slow dynamical regime close to the many-body localization transition, Phys. Rev. B **93**, 060201 (2016).

[10] J. Eisert and T. J. Osborne, General Entanglement Scaling Laws from Time Evolution, Phys. Rev. Lett. **97**, 150404 (2006).

[11] G. D. Chiara, S. Montangero, P. Calabrese, and R. Fazio, Entanglement entropy dynamics of Heisenberg chains, J. Stat. Mech.: Theor. Exp. (2006) P03001.

[12] M. Žnidarič, T. Prosen, and P. Prelovšek, Many-body localization in the Heisenberg *xxz* magnet in a random field, Phys. Rev. B **77**, 064426 (2008).

[13] J. H. Bardarson, F. Pollmann, and J. E. Moore, Unbounded Growth of Entanglement in Models of Many-Body Localization, Phys. Rev. Lett. **109**, 017202 (2012).

[14] R. Nandkishore and D. A. Huse, Many-body localization and thermalization in quantum statistical mechanics, Annu. Rev. Condens. Matter Phys. **6**, 15 (2015).

[15] R. Vasseur and J. E. Moore, Nonequilibrium quantum dynamics and transport: from integrability to many-body localization, J. Stat. Mech.: Theor. Exp. (2016) 064010.

[16] G. De Tomasi, S. Bera, J. H. Bardarson, and F. Pollmann, Quantum Mutual Information as a Probe for Many-Body Localization, Phys. Rev. Lett. **118**, 016804 (2017).

[17] S. Bera and A. Lakshminarayan, Local entanglement structure across a many-body localization transition, Phys. Rev. B **93**, 134204 (2016).

[18] J. Goold, C. Gogolin, S. R. Clark, J. Eisert, A. Scardicchio, and A. Silva, Total correlations of the diagonal ensemble herald the many-body localization transition, Phys. Rev. B **92**, 180202 (2015).

[19] S. Campbell, M. J. Power, and G. De Chiara, Dynamics and asymptotics of correlations in a many-body localized system, Eur. Phys. J. D **71**, 206 (2017).

[20] S. L. Braunstein and C. M. Caves, Statistical Distance and the Geometry of Quantum States, Phys. Rev. Lett. **72**, 3439 (1994).

[21] W. K. Wootters, Statistical distance and Hilbert space, Phys. Rev. D **23**, 357 (1981).

[22] L. Pezzé and A. Smerzi, Entanglement, Nonlinear Dynamics, and the Heisenberg Limit, Phys. Rev. Lett. **102**, 100401 (2009).

[23] P. Hyllus, W. Laskowski, R. Krischek, C. Schwemmer, W. Wieczorek, H. Weinfurter, L. Pezzé, and A. Smerzi, Fisher information and multiparticle entanglement, Phys. Rev. A **85**, 022321 (2012).

[24] G. Tóth, Multipartite entanglement and high-precision metrology, Phys. Rev. A **85**, 022322 (2012).

[25] M. A. Rajabpour, Multipartite entanglement and quantum Fisher information in conformal field theories, Phys. Rev. D **96**, 126007 (2017).

[26] M. Gabbrielli, A. Smerzi, and L. Pezzè, Multipartite entanglement at finite temperature, Sci. Rep. **8**, 15663 (2018).

[27] P. Hauke, M. Heyl, L. Tagliacozzo, and P. Zoller, Measuring multipartite entanglement through dynamic susceptibilities, Nat. Phys. **12**, 778 (2016).

[28] J. Ma and X. Wang, Fisher information and spin squeezing in the Lipkin-Meshkov-Glick model, Phys. Rev. A **80**, 012318 (2009).

[29] T.-L. Wang, L.-N. Wu, W. Yang, G.-R. Jin, N. Lambert, and F. Nori, Quantum Fisher information as a signature of the superradiant quantum phase transition, New J. Phys. **16**, 063039 (2014).

[30] R. H. Dicke, Coherence in spontaneous radiation processes, Phys. Rev. **93**, 99 (1954).

[31] P. Kirton, M. M. Roses, J. Keeling, and E. G. D. Torre, Introduction to the Dicke model: From equilibrium to nonequilibrium, and vice versa, Adv. Quantum Technologies **2**, 1800043 (2018).

[32] A. Altland and F. Haake, Quantum Chaos and Effective Thermalization, Phys. Rev. Lett. **108**, 073601 (2012).

[33] A. Altland and F. Haake, Equilibration and macroscopic quantum fluctuations in the Dicke model, New J. Phys. **14**, 073011 (2012).

[34] C. Emary and T. Brandes, Chaos and the quantum phase transition in the Dicke model, Phys. Rev. E **67**, 066203 (2003).

[35] C. W. Helstrom, Quantum detection and estimation theory, J. Stat. Phys. **1**, 231 (1969).

[36] L. J. Fiderer and D. Braun, Quantum metrology with quantum-chaotic sensors, Nat. Commun. **9**, 1351 (2018).

[37] B. Lücke, M. Scherer, J. Kruse, L. Pezzé, F. Deuretzbacher, P. Hyllus, O. Topic, J. Peise, W. Ertmer, J. Arlt, L. Santos, A. Smerzi, and C. Klempt, Twin matter waves for interferometry beyond the classical limit, Science **334**, 773 (2011).

[38] H. Strobel, W. Muessel, D. Linnemann, T. Zibold, D. B. Hume, L. Pezzè, A. Smerzi, and M. K. Oberthaler, Fisher information and entanglement of non-gaussian spin states, Science **345**, 424 (2014).

[39] F. Fröwis, P. Sekatski, and W. Dür, Detecting Large Quantum Fisher Information with Finite Measurement Precision, Phys. Rev. Lett. **116**, 090801 (2016).

[40] L. Pezzè, Y. Li, W. Li, and A. Smerzi, Witnessing entanglement without entanglement witness operators, Proc. Natl. Acad. Sci. USA **113**, 11459 (2016).

[41] I. Apellaniz, M. Kleinmann, O. Gühne, and G. Tóth, Optimal witnessing of the quantum Fisher information with few measurements, Phys. Rev. A **95**, 032330 (2017).

[42] T. Gorin, T. Prosen, T. H. Seligman, and M. Žnidarič, Dynamics of Loschmidt echoes and fidelity decay, Phys. Rep. **435**, 33 (2006).

[43] T. Prosen, T. H. Seligman, and M. Žnidarič, Evolution of entanglement under echo dynamics, Phys. Rev. A **67**, 042112 (2003).

[44] The fact that the asymptotic value of the QFI is larger in the ergodic phase was already observed in Ref. [54].

[45] In the case of the double-plateau, the fit starts from the fixed point at the end of the first plateau.

[46] G. S. Agarwal, Relation between atomic coherent-state representation, state multipoles, and generalized phasespace distributions, Phys. Rev. A **24**, 2889 (1981).

[47] A. R. Edmonds, *Angular Momentum in Quantum Mechanics* (Princeton University Press, Princeton, New Jersey, 2016).

[48] W. H. Zurek, Sub-planck structure in phase space and its relevance for quantum decoherence, Nature (London) **412**, 712 (2001).

[49] J. Smith, A. Lee, P. Richerme, B. Neyenhuis, P. W. Hess, P. Hauke, M. Heyl, D. A. Huse, and C. Monroe, Many-body localization in a quantum simulator with programmable random disorder, Nat. Phys. **12**, 907 (2016).

[50] S. Krämer, D. Plankensteiner, L. Ostermann, and H. Ritsch, QuantumOptics.jl: A julia framework for simulating open quantum systems, Comput. Phys. Commun. **227**, 109 (2018).

[51] QuantumOptics.jl, https://qojulia.org

[52] M. Kitagawa and M. Ueda, Squeezed spin states, Phys. Rev. A **47**, 5138 (1993).

[53] V. Giovannetti, S. Lloyd, and L. Maccone, Quantum-enhanced measurement: Beating the standard quantum limit, Science **306**, 1330 (2004).

[54] L. Song, J. Ma, D. Yan, and X. Wang, Quantum Fisher information and chaos in the Dicke model, Eur. Phys. J. D **66**, 201 (2012).